

Special Focus

Automated quantitative analysis of epithelial cell scatter

Melissa D. Pope,¹ Nicholas A. Graham,^{2,†} Beijing K. Huang² and Anand R. Asthagiri^{2,*}

¹Division of Engineering and Applied Science; ²Division of Chemistry and Chemical Engineering; California Institute of Technology; Pasadena, California USA

[†]Present address: Crump Institute for Molecular Imaging; University of California; Los Angeles, California USA

Abbreviations: EMT, epithelial-mesenchymal transition; EGF, epidermal growth factor; GM, growth medium; CT, cholera toxin; SFM, serum-free medium

Key words: cell scatter, EMT, automated image analysis

Epithelial cell scatter is a well-known *in vitro* model for the study of epithelial-mesenchymal transition (EMT). Scatter recapitulates many of the events that occur during EMT, including the dissociation of multicellular structures and increased cell motility. Because it has been implicated in tumor invasion and metastasis, much effort has been made to identify the molecular signals that regulate EMT. To better understand the quantitative contributions of these signals, we have developed metrics that quantitatively describe multiple aspects of cell scatter. One metric (cluster size) quantifies the disruption of intercellular adhesions while a second metric (nearest-neighbor distance) quantifies cell dispersion. We demonstrate that these metrics delineate the effects of individual cues and detect synergies between them. Specifically, we find epidermal growth factor (EGF), cholera toxin (CT) and insulin to synergistically reduce cluster sizes and increase nearest-neighbor distances. To facilitate the rapid measurement of our metrics from live-cell images, we have also developed automated techniques to identify cell nuclei and cell clusters in fluorescence images. Taken together, these studies provide broadly applicable quantitative image analysis techniques and insight into the control of epithelial cell scatter, both of which will contribute to the understanding of EMT and metastasis.

Introduction

Epithelial cells have an intrinsic ability to self-assemble into multicellular structures. For example, submandibular gland (SMG) epithelial cells isolated from embryonic mice retain the ability to self-organize into branched tissue aggregates in a manner analogous to that which occurs *in vivo*.¹ These epithelial tissues have a distinct, well-ordered structure. Namely, constituent cells tightly adjoin to their neighbors and form highly polarized multicellular sheets that provide physical barriers between external and internal environments. In addition, epithelial cells are motile, in that they

can move away from their neighbors, but generally remain within the epithelial layer.²

Many epithelial tissues are dynamic structures that undergo constant regeneration. Disruptions in the self-assembly and maintenance of epithelial cell structures can have drastic pathological consequences such as cancer development.³ These physical disruptions are driven by molecular perturbations that alter cell behavior. For example, oncogenes such as *c-met* break up cellular aggregates and promote cell dispersion.⁴ At a single cell level, these molecular perturbations induce an epithelial-mesenchymal transition (EMT). During EMT, epithelial cells lose apical-basolateral polarity and transform into a more migratory phenotype, resembling fibroblasts. This allows cells to dissociate from the epithelial layer and disperse.⁵

Because of the clinical and physiological significance of EMT, much effort has been made to identify the molecular signals that control this process. An important tool for the *in vitro* study of EMT is the cell scatter assay, in which two-dimensional epithelial aggregates dissociate in response to extracellular stimuli. While advances are being made in cataloguing the signaling pathways that control scatter, an emerging challenge is to understand the quantitative contributions of these signals and any coupling between them. For example, which stimuli are the most potent effectors? Which signals work synergistically? Which signals work antagonistically?

A challenge to answering these questions is that current studies of cell scatter are largely qualitative. Prevalent in the limited quantitative literature are studies that score cellular aggregates as “scattered” based on an observed morphological change—for example the appearance of space between cells, the disappearance of membrane-localized desmoplakin or a reduction in the number of cell-cell adhesions.⁶⁻⁹ Such analyses permit comparison between experimental conditions but provide little insight into the cellular-level response.

In this work, we introduce quantitative metrics to systematically characterize multiple aspects of epithelial cell scatter. One metric is the aggregate size, which quantifies the degree to which cells have disrupted intercellular adhesions. Another metric is the distance between a cell and its nearest neighbor, which evaluates the extent to which cells disperse. Our data shows that these metrics delineate the effects of individual molecular signals and detect synergies between them. Specifically, we find epidermal growth factor (EGF) to be

*Correspondence to: Anand R. Asthagiri; 1200 E. California Blvd MC 210-41; Pasadena, California 91125 USA; Tel.: 626.395.8130; Fax: 626.568.8743; Email: anand@cheme.caltech.edu

Submitted: 02/18/08; Accepted: 05/01/08

Previously published online as a *Cell Adhesion & Migration* E-publication: <http://www.landesbioscience.com/journals/celladhesion/article/6218>

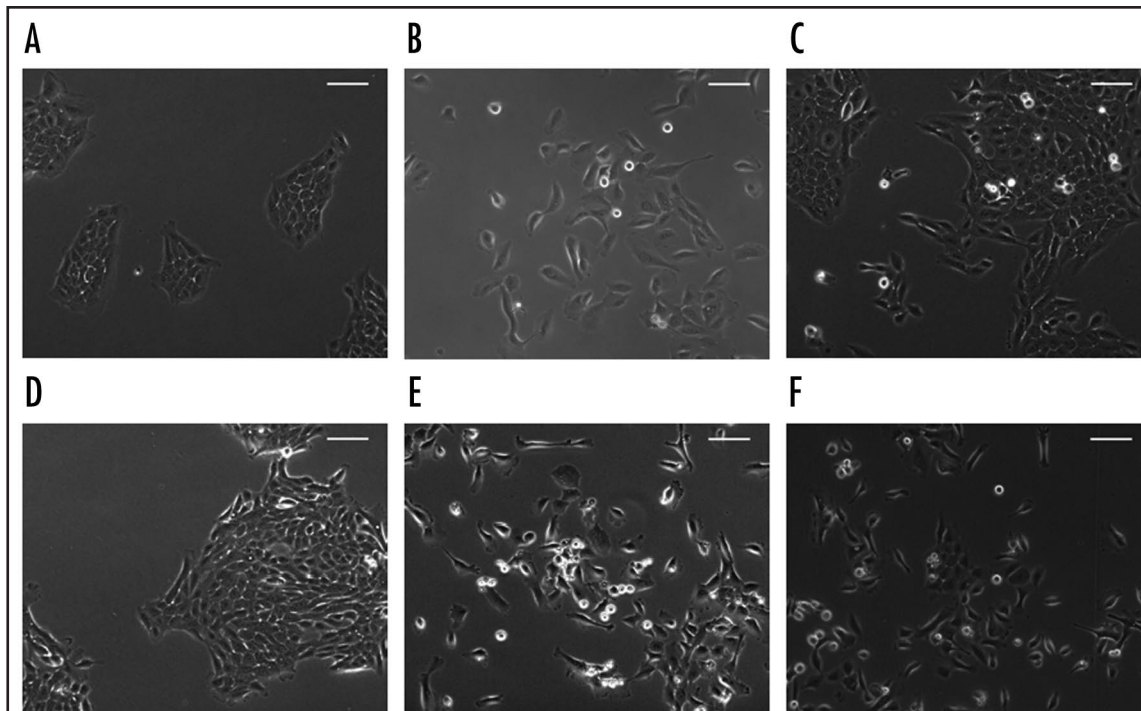


Figure 1. EGF is a key regulator of epithelial cell scatter. (A) MCF-10A cells were maintained in SFM for 24 hours to induce the formation of multicellular aggregates. To induce scatter, aggregates were then treated for 24 hours with multiple soluble factors. GM (B), EGF + CT (E) and EGF + CT + insulin (F) induce cell scatter, while EGF (D) and GM containing all factors except for EGF (C) do not. EGF, CT and insulin were used at concentrations identical to those of GM: 20 ng/ml, 100 ng/ml and 10 μ g/ml respectively. Scale bars are 100 μ m.

essential for scattering non-transformed human mammary epithelial cells (MCF-10A) and to synergize with both cholera toxin (CT) and insulin to reduce aggregate sizes and increase internuclear distances. To facilitate the rapid measurement of our metrics from live-cell images, we have also developed automated techniques to identify cell nuclei and multicellular aggregates in fluorescence images. In summary, this work provides an experimental methodology and high throughput techniques that will prove useful for gleaning quantitative insights into EMT.

Results

EGF regulates MCF-10A scatter. When deprived of the soluble factors contained in growth medium (GM), MCF-10A cells aggregate into well-defined clusters (Fig. 1A). Upon re-addition of GM, cells scatter (Fig. 1B). GM has several components, among them EGF, which has been shown to induce scatter in multiple cell lines.^{7,8,10,11} When EGF is omitted from GM, cell scatter is noticeably reduced (Fig. 1C). However, EGF alone is unable to induce scatter (Fig. 1D). Therefore, EGF appears to be required for scatter but not sufficient to induce a response. We next performed a qualitative screen to identify additional components of GM that contribute to scatter. Among them were CT and insulin. CT appears to synergize with EGF to induce scatter (Fig. 1E), while the further addition of insulin makes little noticeable enhancement (Fig. 1F) even after comparing across 16 different fields (Suppl. Data). Thus, based on this qualitative analysis, we conclude that (1) although EGF is essential for cell scatter, it alone does not induce cell scatter, and (2) CT, but not insulin, significantly synergizes with EGF to induce cell scatter. To test these assessments more rigorously, we sought to quantify the extent of cell scatter induced by these different treatments.

Quantitative metrics of cell scatter. We propose two metrics to quantify the extent of cell scatter. The first metric is the number of cells in a cluster, i.e., the cluster size. A cell cluster is defined as a group of cells in which every member is in physical contact with at least one other member. This metric quantifies the degree to which cells have disrupted intercellular adhesions. Therefore, the mean cluster size is expected to decrease as cells scatter. This metric would not, however, effectively gauge the degree to which cells have dispersed. Thus, a loosely disaggregated cluster would score equivalently to a completely scattered population. To address this issue, we propose a second metric, the nearest-neighbor distance, to evaluate cell dispersion. The nearest-neighbor distance measures the distance between a cell and its nearest neighbor. We expect the mean nearest-neighbor distance to increase as cells scatter. This metric of cell scatter would have a lower limit (the diameter of a single cell) and an upper limit that depends on the surface density of cells.

The distribution of cluster sizes is differentially altered by EGF-containing media. After serum-starvation, the distribution of cluster sizes is bimodal, with one peak centered at small sizes (2–5 cells per cluster) and a second peak centered at moderate sizes (20–30 cells per cluster) (Fig. 2A). Upon treatment with EGF for 24 hours, the fraction of isolated cells (i.e. 1 cell per cluster) remains unchanged. This confirms that EGF is not sufficient to disrupt multicellular aggregates (Fig. 1D). However, unexpectedly, treatment with EGF dramatically reduces the fraction of cells in small- and moderate-sized clusters (2–70 cells per cluster), leading to the emergence of a new population of large aggregates (100+ cells per cluster) (Fig. 2B).

This observation from our quantitative measurements led us to probe several mechanisms that may underlie these changes.

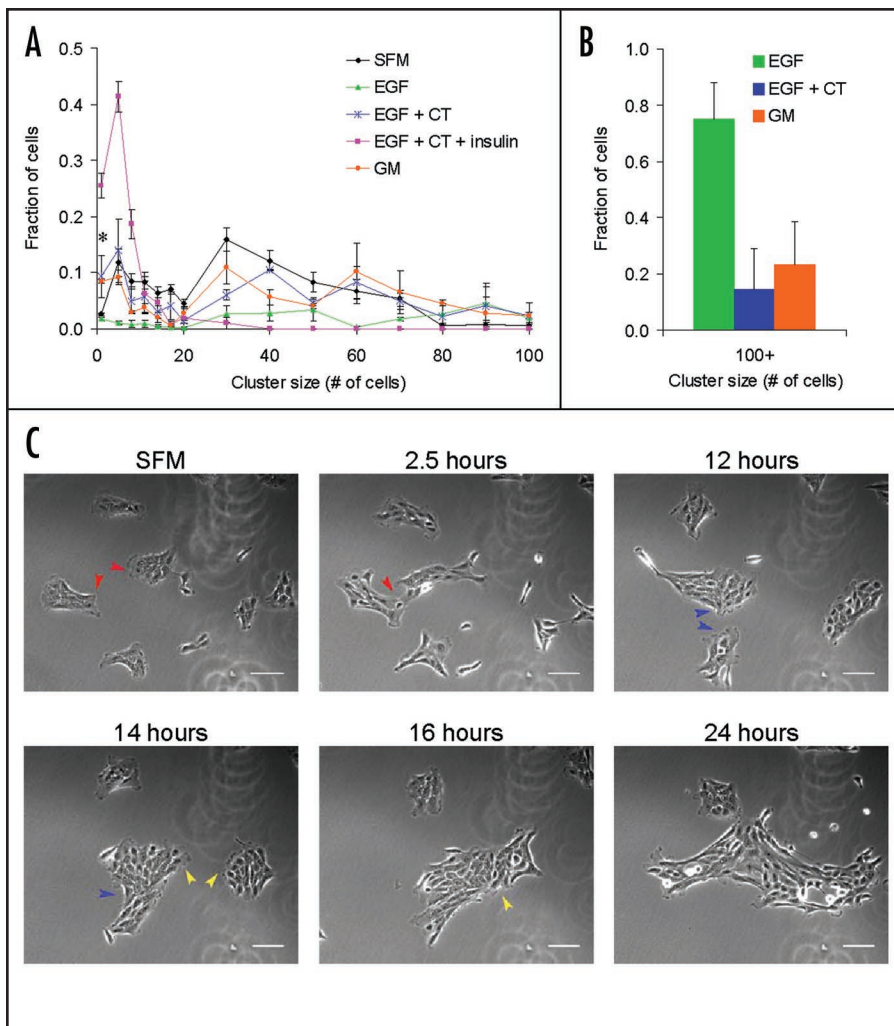


Figure 2. Distribution of cluster sizes for scattering cells. MCF-10A cells were maintained in SFM for 24 hours to induce the formation of multicellular aggregates. (A and B) Aggregates were treated with the indicated factor(s) for 24 hours to induce scatter. 15–30 epifluorescence images were acquired per condition per experiment and cluster size was determined for all clusters completely contained within an image (150–250 clusters per condition per experiment). EGF, EGF + CT and GM induce the formation of large aggregates (100+ cells per cluster) while SFM and EGF + CT + insulin do not. Note that since the fraction of cells in aggregates of 100+ cells is equal to zero for the SFM and EGF + CT + insulin conditions, they are not included in Figure 2B. Data are means \pm standard error; $n = 3$. Asterisk denotes $p < 0.05$ (Student's *t* test) in comparing the fraction of cells that are isolated after treatment with EGF + CT to the fraction of cells that are isolated after culture in SFM and comparing the fraction of cells that are isolated after treatment with GM to the fraction of cells that are isolated after culture in SFM. (C) Aggregates were treated with EGF and imaged via time-lapse microscopy for 24 hours. Arrowheads indicate locations where new adhesions are formed. Scale bars are 100 μm .

One possibility is that proliferation within small- and moderate-sized aggregates causes an increase in cluster size. Because MCF-10A proliferation occurs on a timescale of 18 hours post-treatment with EGF, we would expect proliferation effects in our experiments to be minimal. Indeed, we find that these large aggregates form even in the presence of aphidicolin, an inhibitor of proliferation (data not shown). A second possibility is that small- and moderate-sized clusters aggregate to form large ones. To test this possibility, we collected time-lapse videos of serum-starved cells treated with EGF. These videos clearly show the amalgamation of small/moderate-sized

aggregates into large aggregates (Fig. 2C). It therefore appears that although EGF is required for scatter, treatment with this factor alone promotes the formation of new cell-cell adhesions and the amalgamation of pre-existing aggregates.

Treatment with CT in conjunction with EGF increases the fraction of cells that are isolated or in small clusters after 24 hours compared to treatment with EGF alone. This result is consistent with the apparent cell scatter induced by co-treatment with EGF and CT (Fig. 1E). Furthermore, inclusion of CT reduces the formation of new large clusters. CT therefore synergizes with EGF in both disrupting cell-cell adhesions and reducing the formation of new adhesions.

The further addition of insulin results in nearly complete dissociation of moderate-sized aggregates (15–100 cells per cluster), and predominantly small clusters and isolated cells remain after 24 hours. Thus, insulin makes a striking contribution to the disruption of cell clusters that was not evident from our qualitative analysis (Fig. 1F). Our quantitative measurements reveal that insulin-mediated signals are essential for maximum scatter.

Notably, GM, which in addition to EGF, CT and insulin contains serum and hydrocortisone, is a less potent promoter of scatter than EGF + CT + insulin. This suggests that additional components contained within GM may counteract insulin-mediated effects and reduce scatter.

The distribution of nearest-neighbor distances is differentially altered by EGF-containing media. After serum-starvation, nearly every cell is a member of an aggregate and therefore in contact with its nearest neighbor. Upon stimulation with EGF-containing media, the fraction of cells in contact with their nearest neighbor (i.e., a nearest-neighbor distance of ≤ 1 cell diameter) decreases (Fig. 3). EGF alone produces little change in the distribution of nearest-neighbor distances. However, the additions of CT and insulin produce stepwise increases in the fraction of cells that have distanced themselves from their neighbors by multiple cell diameters. GM induces the greatest response, scattering a small population of cells by greater than two cell diameters.

To determine if the measured nearest-neighbor distances approach those expected at maximal scatter, we calculated a theoretical maximum internuclear distance that corresponds to the case where all cells are equally spaced from one another. This distance was calculated as follows: the surface area contained within an image was divided by the number of cells within the image to determine an area per cell. Assuming each cell to be a circle of the resulting area with a nucleus at its center, the maximum internuclear distance was

calculated to be $76.9 \pm 4.8 \mu\text{m}$ or ~ 1.8 cell diameters. Therefore, the distances presented in Figure 3 approach the values expected at the time of maximal scatter.

Automated image processing. From the data presented above, it is clear that our metrics provide useful quantitative insight into the regulation of epithelial cell scatter and exhibit promise for use in future studies. The manual measurement of these metrics, however, is time-consuming. We have therefore developed a simple, high throughput method for identifying cell nuclei and multicellular aggregates in fluorescence images.

MCF-10A cells expressing nuclear-localized GFP and membrane-localized mCherry were imaged using epifluorescence and a digital CCD camera (Fig. 4A and A'). GFP-channel intensity images were segmented using the MATLAB function `edge`. `Edge` creates a binary image with 1's where the function finds edges and 0's elsewhere. Next, the function `imfill` was used to fill holes (areas of black pixels surrounded by white pixels) in the segmented images (Fig. 4B). This algorithm correctly reconstructs isolated nuclei, but fails to resolve contacting nuclei into distinct structures. In fact, contact between nuclei is occasionally created by under-segmentation. To address this issue, the watershed algorithm was applied to the image and successfully divides overlapping nuclei into distinct objects.¹²

To identify cell clusters, a global threshold was applied to red-channel intensity images using the MATLAB function `graythresh`. `Graythresh` computes a global threshold for each image using Otsu's algorithm.¹³ This method correctly identifies all cell clusters, but also introduces additional small objects into the image. To eliminate these non-cellular components, a size threshold was applied to the image using the function `bwareopen`. Objects smaller than the area of a single cell ($\sim 400 \mu\text{m}^2$) were eliminated from the image, resulting in a binary image containing distinct cell clusters (Fig. 4B').

Cluster size and nearest-neighbor distance metrics were easily and quickly extracted from the processed images. To determine cluster sizes, clusters in membrane-mCherry frames were first indexed using the function `bwlabel`. `Bwlabel` creates a matrix in which pixels labeled 0 make up the background, pixels labeled 1 make up one object, pixels labeled 2 make up a second object, and so on. From each indexed image, a series of masks was created such that each mask contained a single cluster (Fig. 4C). Masks were then applied to the corresponding H2B-GFP image and the nuclei overlapping with each were indexed and counted using `bwlabel` (Fig. 4C'). To determine nearest-neighbor distances, nuclear centroids were determined from the segmented H2B-GFP frames using the function `regionprops`. Internuclear distances were calculated and the minimum distance measured for each cell was recorded.

We next performed a trial experiment to determine the precision with which these automated techniques evaluate our metrics. Scattering MCF-10A cells co-expressing H2B-GFP and membrane-mCherry were imaged via phase contrast and epifluorescence. Cluster sizes and nearest-neighbor distances were determined (1) manually from phase contrast images and (2) from fluorescence images of the same fields using the described automated method. For both the SFM and GM conditions, results obtained via automated image processing were similar to those obtained manually (Fig. 5).

We note that for each application (i.e., cell line and stimulation conditions), one must also test whether the H2B-GFP and

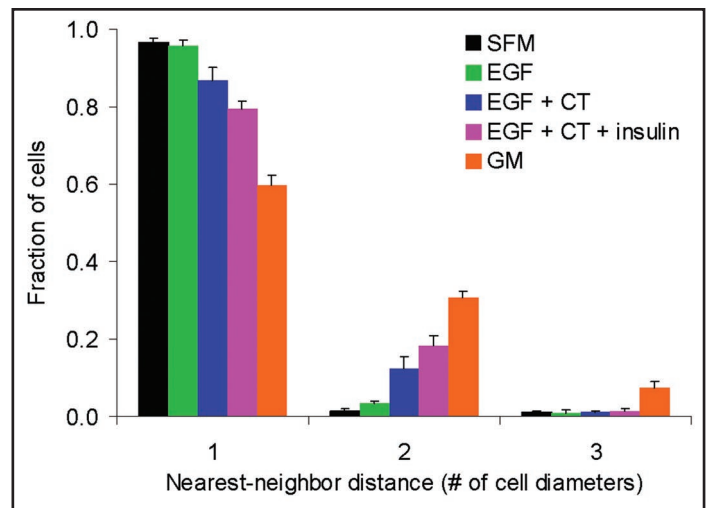


Figure 3. Distribution of nearest-neighbor distances for scattering cells. MCF-10A cells were maintained in SFM for 24 hours to induce the formation of multicellular aggregates. Aggregates were then treated with the indicated factor(s) and imaged via time-lapse microscopy for 24 hours. Nearest-neighbor distances were determined for all cells within the first (SFM) and last frames. A cell diameter was taken to be the greatest nearest-neighbor distance measured for contacting serum-starved cells ($42 \mu\text{m}$), and all nearest-neighbor distances were expressed as multiples of this distance. Data are means \pm standard error; $n = 2$.

membrane-mCherry constructs perturb cell behavior. This is best accomplished by comparing cluster sizes and nearest-neighbor distances determined manually for uninfected cells to those determined manually for cells expressing the fluorescent constructs.

Discussion

Epithelial organization is regulated by a complex signaling network. Many scatter-promoting factors have been identified, among them EGF, hepatocyte growth factor (HGF), fibroblast growth factor (FGF) and transforming growth factor β (TGF β). These extracellular cues trigger various intracellular signals—Src, Rac, PI3K and Erk, for example—that drive scatter.^{3,14,15} A key limiting factor in our understanding of this phenomenon is that the phenotypic changes associated with scatter are characterized largely in qualitative terms. Such assessment is inadequate for several reasons. First, qualitative characterizations do not provide insight into how important a particular factor might be. Is the degree of scatter induced by EGF the same as that induced by HGF? Is there quantitative synergy when both signals are received? Second, cell scatter is a complex phenomenon involving several events. These events include de-compaction of the aggregate, cell-cell dissociation and cell migration. However, because cell scatter is currently evaluated in a lumped fashion, the precise facet(s) of cell scatter a given signal affects remain unclear.

This work introduces quantitative metrics to describe multiple aspects of epithelial cell scatter. We demonstrate that these metrics gauge the potencies with which specific signals induce scatter and the synergies among them. Our measurements show that although EGF alone is unable to induce cell scatter, it synergizes with CT to reduce aggregate sizes and increase nearest-neighbor distances. Furthermore,

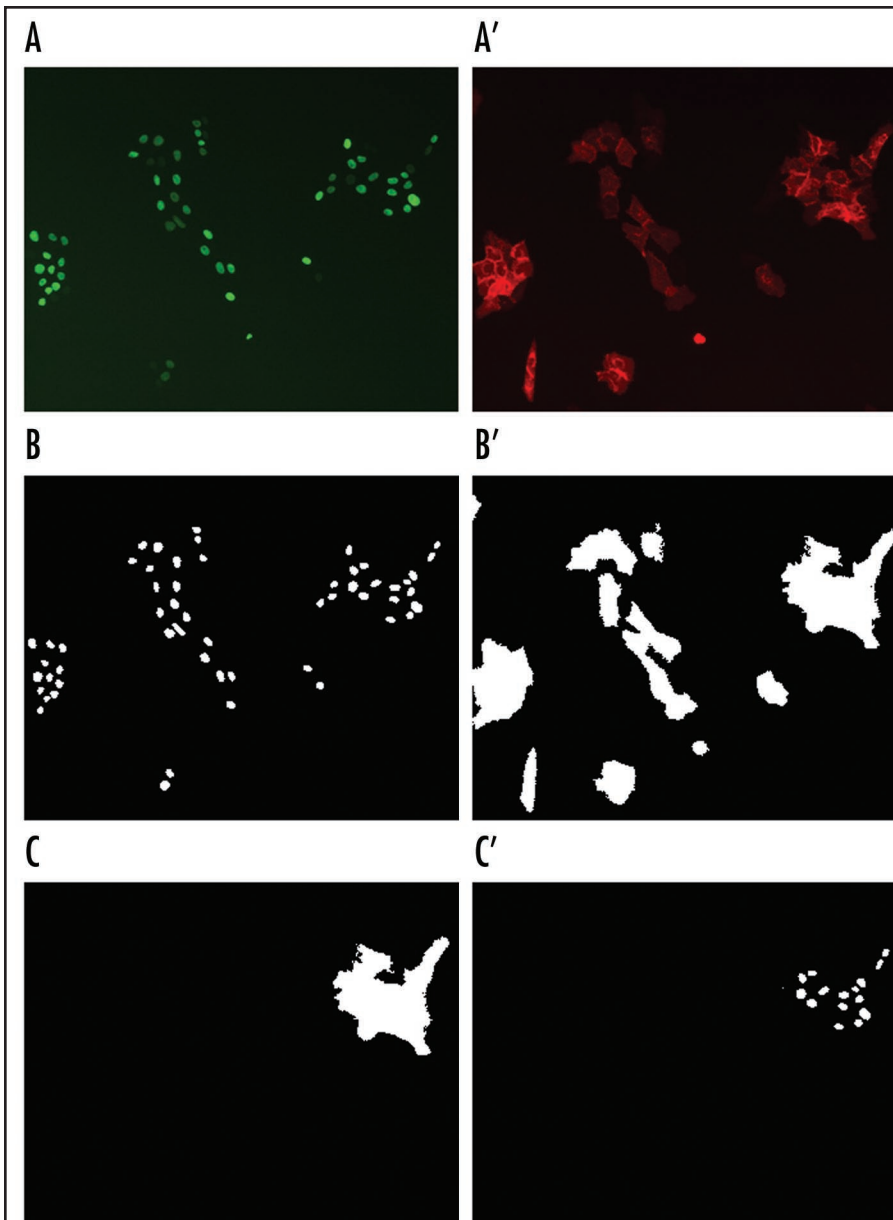


Figure 4. Automated image processing using MATLAB. (A and A') Nuclear- and membrane-localized fluorescent proteins, H2B-GFP and mCherry respectively, were co-expressed in MCF-10A cells. (B and B') Epifluorescence images of scattering cells were segmented using thresholding and edge detection algorithms in MATLAB. (C) Masks were created such that each mask contained a single cluster. (C') Masks were then applied to the corresponding H2B-GFP image and nuclei that co-localized with the mask were identified. These nuclei were counted to determine the cluster size.

our quantitative metrics extracted information regarding the role of insulin that would be missed from a qualitative analysis. Inspecting images of cells treated with EGF, CT and insulin suggested that insulin provided no major enhancement to the scatter induced by EGF and CT. However, quantitative measurements of cluster sizes and nearest-neighbor distances revealed that insulin provides a striking improvement in cell scatter, essentially ablating all clusters. This type of quantitative analysis will prove useful for categorizing scatter-promoting factors according to their ability to alter epithelial structures and for grouping synergistic cues. Moreover, identifying

potent scatter-inducing cues may provide more pivotal targets for anti-cancer therapeutics.

This quantitative approach also provides new insights into the role of EGF in multicellular epithelial organization. Our measurements revealed that treatment with EGF alone induced the formation of large aggregates through the amalgamation of small/moderate-sized aggregates. Thus, although EGF is essential for inducing cell scatter in the presence of co-factors, our data suggest that EGF alone promotes cell-cell adhesion and the emergence of large clusters.

The metrics presented in this study quantify distinct aspects of scatter, and therefore, may not always be correlated to each other. For example, GM treatment does not score as the most efficient at breaking clusters apart (Fig. 2), but still mediates the largest increase to nearest-neighbor distance (Fig. 3). This counterintuitive observation is due to a phenomenon called de-compaction, where cells in a cluster relax cell-cell adhesions and enhance cell spreading against the substratum. In this manner, GM-treated cells distance themselves from their neighbors without breaking cell-cell contacts. Thus, the proposed metrics gauge distinct aspects of multicellular organization and analyzing how both metrics respond to molecular perturbations can provide mechanistic insights.

Because the metrics capture distinct facets of cell scatter, they will also prove useful in exploring synergisms between signals. Some cues, for instance, will have a profound effect on breaking cell-cell contacts but little effect on the nearest-neighbor distance. Other cues will have exactly the opposite effect. Combined exposure to such complementary cues may have a synergistic effect on cell scatter that is significantly greater than their individual contributions. Identifying such synergistic cues may reveal “multi-hit” pathways that contribute to cancer development and thereby guide therapeutic strategies.

In this work, we also present a simple, versatile and high-throughput method for measuring morphological changes to epithelial structures from live-cell images. These techniques may be a valuable tool not only for in-depth study of cell

scatter, but also for clinical applications. First, quantitative metrics combined with automated image analysis may facilitate *in vitro* high-throughput screening of anti-cancer therapeutics. Furthermore, since inspection of tumor morphology is widely used to categorize disease and decide on a treatment option, the techniques described here may facilitate advancements in cancer diagnostics.^{3,5} Overall, we believe our methods can provide necessary quantitative insight into the regulation of epithelial structures, which will lead to advancements in our understanding of scatter, EMT and metastasis.

Materials and Methods

Cell culture. MCF-10A cells were cultured in Dulbecco's modified Eagle's medium/Ham's F-12 containing HEPES and L-glutamine (Invitrogen) supplemented with 5% (v/v) horse serum (Invitrogen), 20 ng/ml EGF (Peprotech), 0.5 µg/ml hydrocortisone (Sigma), 0.1 µg/ml cholera toxin (Sigma), 10 µg/ml insulin (Sigma) and 1% penicillin/streptomycin (Invitrogen). For serum starvation, cells were washed twice with PBS and then cultured in Dulbecco's modified Eagle's medium/Ham's F-12 supplemented with 1% (v/v) penicillin/streptomycin and 0.1% bovine serum albumin (Sigma) for 24 h.

Plasmid constructs. H2B-GFP and membrane-mCherry were gifts from S. Fraser (California Institute of Technology). The membrane-mCherry construct consists of monomeric mCherry fused to the first 20 amino acids of zebrafish Gap43.¹⁶ Palmitoylation at cysteine residues within the Gap43 sequence directs the mCherry protein to the membrane.^{17,18} VSV-G and gag-pol vectors were gifts from D. Schaffer (University of California, Berkeley).

Retroviral infection. H2B-GFP and membrane-mCherry genes were subcloned into retroviral vectors (pLHCX and pLPCX respectively) and expressed in epithelial cell lines via retroviral infection. Retrovirus was produced by triple transfection of 293T cells with 5 µg each of VSV-G, gag-pol and the retroviral vector using LipofectAMINE (Invitrogen). For infection, cells were incubated with retrovirus-containing medium and 8 µg/ml polybrene for 24 h. Puromycin (2 µg/mL) and hygromycin (100 µg/mL) were used for selection.

Cell scatter assay. MCF-10A cells were seeded in GM at a density of 8×10^4 per 35 mm culture dish and, 18–24 hours later, serum starved for 24 hours to induce aggregate formation. Cell aggregates were then stimulated with the indicated factor(s) and imaged. MCF-10A cells co-expressing membrane-mCherry and H2B-GFP were seeded at 2×10^4 per 35 mm dish.

Live cell microscopy. Images were captured at 10x magnification using a Zeiss Axiovert 200 M microscope equipped with a digital CCD camera. Time-lapse microscopy experiments were performed using an environmental chamber that maintains temperature, humidity and CO₂ levels.

Acknowledgements

The authors thank the members of the Asthagiri lab for helpful discussions. Funding for this work was provided by the Concern Foundation for Cancer Research and The Jacobs Institute for Molecular Engineering for Medicine. N.A.G. was supported by a National Defense Science and Engineering Graduate Fellowship; M.D.P. was supported by a National Science Foundation Graduate Fellowship and an NIH Molecular Cell Biology Training Grant (NIH/NRSA5T32GM07616Z).

Note

Supplementary materials can be found at:
www.landesbioscience.com/supplement/PopeCAM2-2-sup.pdf

References

- Wei C, Larsen M, Hoffman MP, Yamada KM. Self-organization and branching morphogenesis of primary salivary epithelial cells. *Tissue engineering* 2007; 13:721-35.
- Schock F, Perrimon N. Molecular mechanisms of epithelial morphogenesis. *Annual review of cell and developmental biology* 2002; 18:463-93.
- Thiery JP. Epithelial-mesenchymal transitions in tumour progression. *Nature reviews* 2002; 2:442-54.

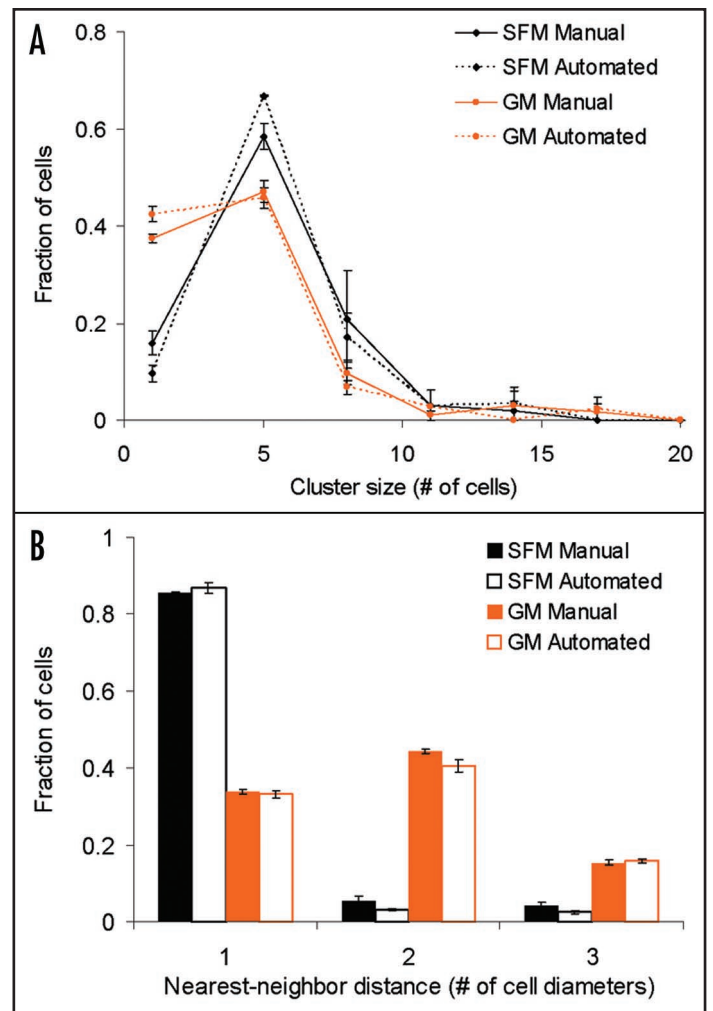


Figure 5. Comparison of manual and automated techniques. MCF-10A cells co-expressing H2B-GFP and membrane-mCherry were maintained in SFM for 24 hours to induce the formation of multicellular aggregates. Aggregates were then treated with GM for 24 hours to induce scatter. For each field, both phase contrast and epifluorescence images were collected. Cluster sizes (A) and nearest-neighbor distances (B) were determined manually from phase contrast images and from epifluorescence images using the described automated techniques. Both cluster size and nearest-neighbor distance distributions are similar for the manual and automated techniques.

- Ma PC, Maulik G, Christensen J, Sargia R. c-Met: structure, functions and potential for therapeutic inhibition. *Cancer metastasis reviews* 2003; 22:309-25.
- Vincent-Salomon A, Thiery JP. Host microenvironment in breast cancer development: epithelial-mesenchymal transition in breast cancer development. *Breast Cancer Res* 2003; 5:101-6.
- Jourquin J, Yang N, Kam Y, Guess C, Quaranta V. Dispersal of epithelial cancer cell colonies by lysophosphatidic acid (LPA). *Journal of cellular physiology* 2006; 206:337-46.
- Boyer B, Roche S, Denoyelle M, Thiery JP. Src and Ras are involved in separate pathways in epithelial cell scattering. *The EMBO journal* 1997; 16:5904-13.
- Edme N, Downward J, Thiery JP, Boyer B. Ras induces NBT-II epithelial cell scattering through the coordinate activities of Rac and MAPK pathways. *Journal of cell science* 2002; 115:2591-601.
- de Rooij J, Kerstens A, Danuser G, Schwartz MA, Waterman Storer CM. Integrin-dependent actomyosin contraction regulates epithelial cell scattering. *The Journal of cell biology* 2005; 171:153-64.
- Lu Z, Ghosh S, Wang Z, Hunter T. Downregulation of caveolin-1 function by EGF leads to the loss of E-cadherin, increased transcriptional activity of beta-catenin, and enhanced tumor cell invasion. *Cancer cell* 2003; 4:499-515.
- Matthay MA, Thiery JP, Lafont F, Stampfer F, Boyer B. Transient effect of epidermal growth factor on the motility of an immortalized mammary epithelial cell line. *Journal of cell science* 1993; 106:869-78.

12. Gonzales R, Woods R, Eddins S. Image Segmentation. In: O'Brian V, ed. Digital Image Processing using MATLAB. Upper Saddle River, NJ: Pearson Prentice Hall 2004.
13. McAndrew A. Image Segmentation. In: Mendelsohn M, ed. Introduction to Digital Image Processing with MATLAB. Boston, MA: Thomson Course Technology 2004.
14. Christofori G. New signals from the invasive front. *Nature* 2006; 441:444-50.
15. Thiery JP, Sleeman JP. Complex networks orchestrate epithelial-mesenchymal transitions. *Nat Rev Mol Cell Biol* 2006; 7:131-42.
16. Shaner NC, Campbell RE, Steinbach PA, Giepmans BN, Palmer AE, Tsien RY. Improved monomeric red, orange and yellow fluorescent proteins derived from *Discosoma* sp. red fluorescent protein. *Nature biotechnology* 2004; 22:1567-72.
17. Skene JH, Virag I. Posttranslational membrane attachment and dynamic fatty acylation of a neuronal growth cone protein, GAP-43. *The Journal of cell biology* 1989; 108:613-24.
18. Zuber MX, Goodman DW, Karns LR, Fishman MC. The neuronal growth-associated protein GAP-43 induces filopodia in non-neuronal cells. *Science (New York, NY)* 1989; 244:1193-5.